RESEARCH ARTICLE SUMMARY

NEUROSCIENCE

Multiscale representation of very large environments in the hippocampus of flying bats

Tamir Eliav†, Shir R. Maimon†, Johnatan Aljadeff, Misha Tsodyks, Gily Ginosar, Liora Las, Nachum Ulanovsky*

INTRODUCTION: Place cells are neurons in the hippocampus that represent the animal's position in space and are important for supporting navigation behaviors. These cells increase their spiking activity when the animal passes through a specific region of space, called the neuron's "place field." Since the discovery of place cells half a century ago, nearly all the research on spatial representations in the mammalian brain has focused on rats and mice as animal models and used small laboratory environments as experimental setups—usually small boxes or short linear tracks ~1 to 2 m in size. In such small environments, individual place cells typically have one place field, with a small field size. However, outdoor navigation of all mammals occurs in natural environments that span much larger spatial scales, of hundreds of meters or kilometers, and nothing is known about the neural codes for such large spatial scales.

RATIONALE: We reasoned that in very large environments, the hippocampus must exhibit a different coding scheme than seen in small environments because large environments cannot be tiled fully by the limited number of hippocampal neurons. We set out to discover this alternative coding scheme and thus to close the longstanding gap between the neurobiology of navigation as studied in the laboratory and natural large-scale navigation. To this end, we studied bats flying in a 200-m-long tunnel while we recorded the activity of hippocampal dorsal CA1 neurons using a custom wireless-electrophysiology system.

RESULTS: We found that place cells recorded in the large environment exhibited a multifield, multiscale representation of space: Individual neurons exhibited multiple place fields of diverse sizes, ranging from <1 m to more than 30 m, and the fields of the same neuron could differ up to 20-fold in size. This multifield, multiscale code was observed already from the first day in the environment and was similar between wild-born and laboratory-born bats that were never exposed to large environments. By contrast, recordings from a small-scale 6-m environment did not reveal such a multiscale code but rather classical single fields. Theoretical decoding analysis showed major advantages of the multiscale code over classical single-field codes, both in the number of required neurons and in the decoding errors. Thus, the multiscale code provides an efficient population code with a high capacity for representing very large environments. We conducted neural-network modeling, which suggested that the multiscale code may arise from interacting attractor networks with multiple scales or from feedforward networks, which yielded experimentally testable predictions for the inputs into CA1.

CONCLUSION: Using this experimental setup, our study uncovered a new coding scheme for large spaces, which was never observed before in small spaces: a multiscale code for space. This coding scheme existed from day 1 in the environment and was observed in both wild-born and laboratory-born bats, suggesting that it does not require previous experience. These findings provide a new notion for how the hippocampus represents space. The large naturalistic scale of our experimental environment was crucial for revealing this type of code. More generally, this study demonstrates the power of studying brain circuits under naturalistic conditions. ■

Question: What is the neural code for very large spaces?

Methods
Bat flying in 200-m-long tunnel with wireless electrophysiology system

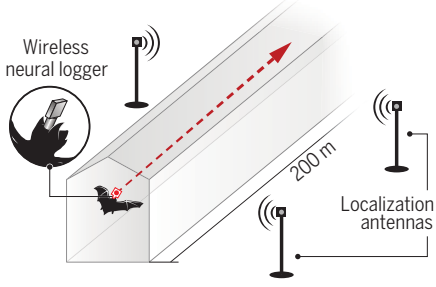

Findings
Individual place-cells in dorsal hippocampus CA1 showed multiple fields with highly variable sizes, from day 1 in the tunnel

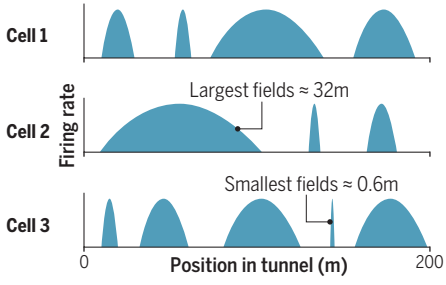

Function
Decoding analysis showed that the multifield multiscale code outperforms classical place-codes

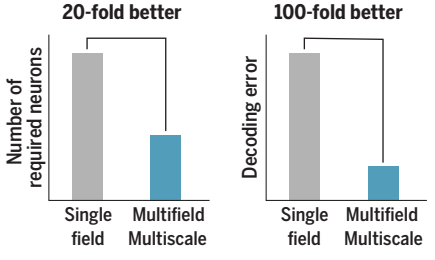

Modeling
Multifield multiscale coding can be explained with 1D interacting attractor networks and feedforward models

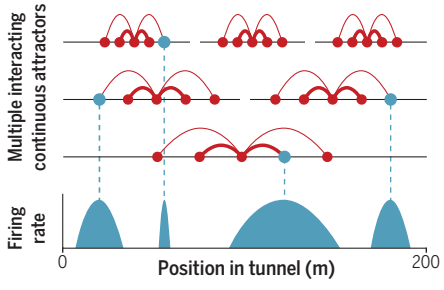

Multiscale hippocampal spatial code for very large environments. (Methods) We wirelessly recorded neural activity from hippocampal neurons of bats flying in a 200-m tunnel. (Findings) Single neurons exhibited multiple place fields with highly heterogeneous field sizes for the same neuron. (Function) This multiscale neural code for space strongly outperforms classical single-field place codes. (Modeling) Modeling by using interacting attractor networks and feedforward models recapitulated the multiscale coding.

The list of author affiliations is available in the full article online.
*Corresponding author. Email: nachum.ulanovsky@weizmann.ac.il
†These authors contributed equally to this work.
Cite this article as T. Eliav *et al.*, *Science* **372**, eabg4020 (2021). DOI: 10.1126/science.abg4020

READ THE FULL ARTICLE AT
https://doi.org/10.1126/science.abg4020

RESEARCH ARTICLE

NEUROSCIENCE

Multiscale representation of very large environments in the hippocampus of flying bats

Tamir Eliav[1]†, Shir R. Maimon[1]†, Johnatan Aljadeff[1,2], Misha Tsodyks[1,3], Gily Ginosar[1], Liora Las[1], Nachum Ulanovsky[1]*

Hippocampal place cells encode the animal's location. Place cells were traditionally studied in small environments, and nothing is known about large ethologically relevant spatial scales. We wirelessly recorded from hippocampal dorsal CA1 neurons of wild-born bats flying in a long tunnel (200 meters). The size of place fields ranged from 0.6 to 32 meters. Individual place cells exhibited multiple fields and a multiscale representation: Place fields of the same neuron differed up to 20-fold in size. This multiscale coding was observed from the first day of exposure to the environment, and also in laboratory-born bats that never experienced large environments. Theoretical decoding analysis showed that the multiscale code allows representation of very large environments with much higher precision than that of other codes. Together, by increasing the spatial scale, we discovered a neural code that is radically different from classical place codes.

Navigation and spatial memory are crucial for the survival of animals in the wild. The hippocampal formation contains several types of spatial neurons whose activity represents the animal's position and direction in space (*1*–*10*). One of these spatial cell types is the "place cell," hippocampal neurons that increase their spiking activity when the animal passes through a specific region of space, in turn called the neuron's "place field" (*1*, *2*, *11*–*15*). Individual place cells typically have only one (or two) place fields in a small environment (*2*, *11*, *16*), whereas multiple place fields are found in dentate-gyrus neurons upstream (*16*). Nearly all of the research on spatial representations in the mammalian brain has focused on rats and mice as animal models and used small laboratory environments as experimental setups—usually small boxes or short linear tracks ~1 to 2 m in size. Consequently, almost all current knowledge on spatial neurons in the hippocampal formation is based on data from animals moving in small laboratory environments. Two studies of place cells examined larger spatial scales (*17*, *18*). However, these studies used either a zig-zagging track composed of ~1-m segments or a track that passed through several small rooms; thus, the largest single-compartment environment in which place cells were recorded to date was <10 m in size.

By contrast, outdoor navigation of all mammals occurs in natural environments that span spatial scales much larger than 10 m. For example, wild rats were shown to navigate outdoors >1 km per night (*19*, *20*). Navigation over such distances requires spatial representation of very large environments, on the scale of hundreds of meters or kilometers (*21*). Egyptian fruit bats fly every night distances of up to ~30 km to their favorite fruit trees, with flyways spanning ~2 km in width and 0.5 km in height (*21*, *22*). A simple calculation shows that tiling this space with typical place fields as measured in the laboratory (~10 to 20 cm diameter, single field per neuron) would require ~10^{13} neurons. This is ~10^{8} times more neurons than the number of cells in the entire dorsal hippocampal area CA1 (*3*), suggesting that it is simply not feasible to represent such large spatial scales with laboratory-sized place fields. Thus, there is a fundamental gap between the neurobiology of navigation as studied in the laboratory and kilometer-scale natural navigation outdoors.

Neural recordings in bats flying in a 200-m environment

We studied wild-born Egyptian fruit bats, a mammal that has rodent-like hippocampal spatial representations in small laboratory environments (*23*–*26*). We developed a miniaturized wireless neural-logging system that stores all the data on board (Fig. 1A). This system enabled neural recordings to be conducted over great distances in freely behaving animals, with uninterrupted experiments lasting up to ~3 hours (*27*). Using this system, we conducted tetrode recordings from dorsal CA1, in flight (Fig. 1, B to D, and fig. S1). We built a 200-m-long flight tunnel (Fig. 1E), composed of a long arm and a shorter arm, with landmarks dispersed along it (fig. S2). We used a medium light level (5 lux), allowing these bats—which have excellent vision (*21*)—to see several distal landmarks from each location in the tunnel (fig. S2B). We used a radio frequency–based localization system, with a small mobile tag placed on the bat that measured the bat's distances to a ground-based antenna array (Fig. 1F). This system yielded a high spatial localization accuracy of ~9 cm (Fig. 1G) along with a high temporal resolution (*27*). We harnessed the natural behavioral tendency of bats to fly long distances in straight trajectories (*22*) and trained them to fly in the tunnel between two landing balls that were placed at the two ends of the tunnel, on which food was given. The bats flew continuously back and forth between the landing balls (fig. S3A). Flight trajectories were rather stereotyped, with bats flying at the center-top portion of the tunnel, with only very small deviations perpendicular to the flight direction (Fig. 1H and fig. S3, B and C). Thus, the bats exhibited nearly perfect one-dimensional (1D) back-and-forth trajectories. Hence, in all subsequent analyses, we projected the behavioral data onto the main axis of the tunnel and included only long unidirectional flights that were >100 m in length (*27*). This 1D tunnel bears similarities to bats' natural behaviors because these bats navigate underground in 1D cave tunnels, and also their flight trajectories outdoors are largely 1D (*22*). Flight speed was high and showed very little variation across different locations (Fig. 1, I and J). Bats flew dozens of flights per direction in each recording session (Fig. 1K), covering on average 14.1 km per session and up to 22.5 km in a single session (Fig. 1L).

Hippocampal place cells exhibit a multifield, multiscale spatial code

We recorded 235 well-isolated putative pyramidal cells from the dorsal CA1 of five bats; all 235 neurons were active in flight, and 83.4% of them (n = 196) were place cells, showing significant spatial tuning with distinct and stable place fields (Fig. 2A and figs. S4 and S5; the numbers of place cells in individual bats are provided in table S1) (*27*). By contrast, in both rodents and bats, the reported percentage of place cells in small environments is typically 30 to 40% of all the recorded cells, whereas the remaining cells are virtually silent during behavior (*11*, *23*, *24*, *28*). Place cells in the 200-m tunnel exhibited strong spatial tuning (Fig. 2, B to D), and the spatial tuning was stable across flights (Fig. 2E). The place cells fired differently in different flight directions (Fig. 2, A, red and blue raster plots, and F, map correlations between directions), similar to the directionality shown previously for place cells in rats and bats in small 1D environments (*29*, *30*). However, we found several surprising characteristics of place cell firing

[1]Department of Neurobiology, Weizmann Institute of Science, Rehovot 76100, Israel. [2]Section of Neurobiology, Division of Biological Sciences, University of California, San Diego, CA 92093, USA. [3]The Simons Center for Systems Biology, Institute for Advanced Study, Princeton, NJ 08540, USA.
*Corresponding author. Email: nachum.ulanovsky@weizmann.ac.il
†These authors contributed equally to this work.

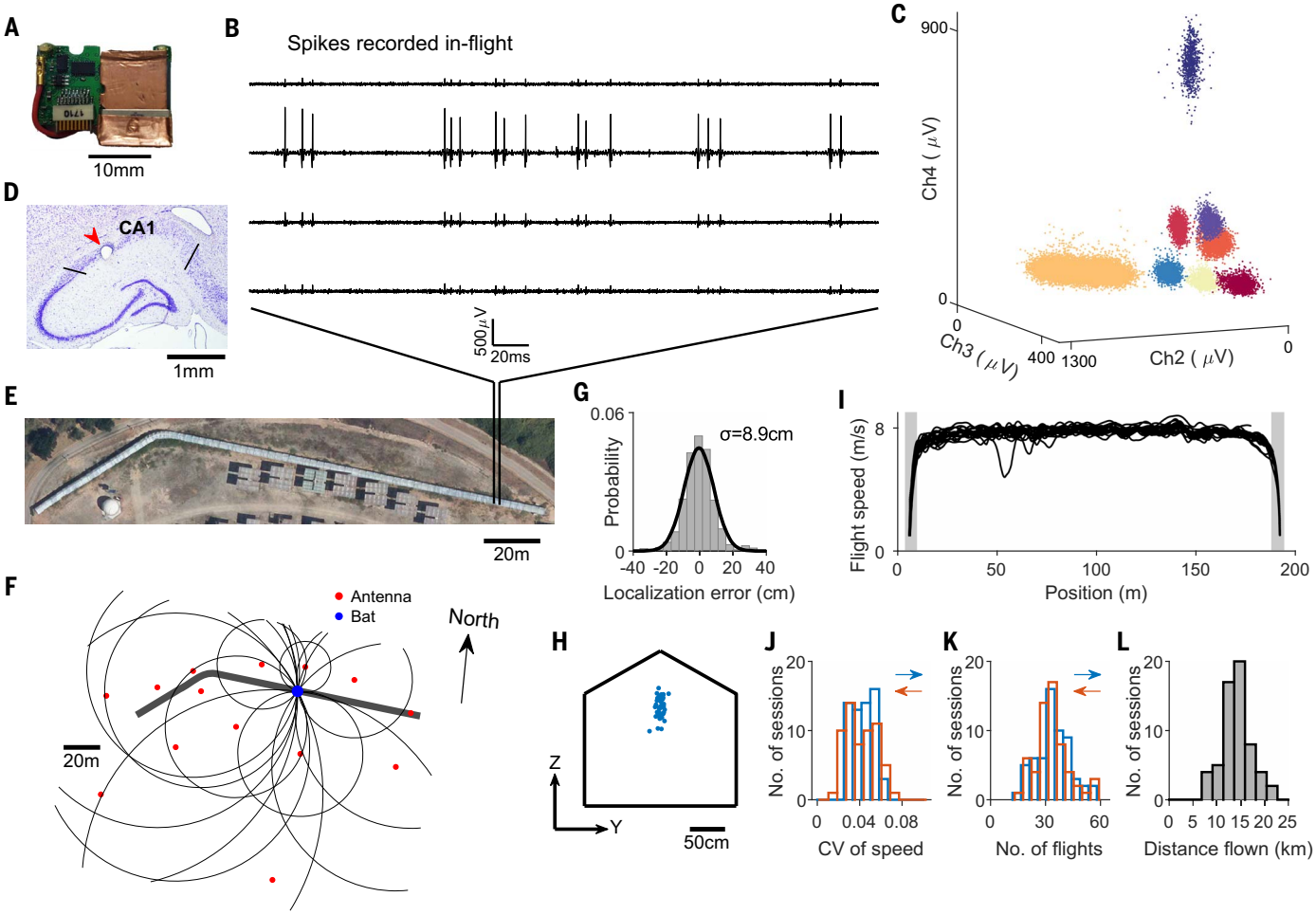

Fig. 1. Neuronal and behavioral recordings from bats flying over large spatial scales. (**A**) Sixteen-channel wireless neural logger. (**B**) Neural traces from one tetrode, recorded in bat dorsal hippocampal area CA1, showing spikes in-flight. (**C**) Spike-sorting of one tetrode (data from full session, 108 min). Shown are spike clusters from different neurons, with spike amplitudes plotted for three of the tetrode's channels; well-isolated units are shown in different colors. Same session and tetrode as in (B). (**D**) Histology of one recording site in dorsal CA1. Red arrowhead, electrolytic lesion; Black lines, proximal and distal borders of CA1. (**E**) Aerial photograph showing top-view of the large-scale environment. The flight-tunnel was composed of long and short arms (*27*), which the bat traversed without slowing down (I). Vertical lines indicate location where neural data in (B) were recorded. (**F**) Localization system, showing positions of ground-based antennas (red dots), the tunnel (dark gray thick line), snapshot of measured distances from each antenna to the localization tag on the bat's head (large black circles; cropped for visualization purposes), and the bat's estimated location (blue dot; computed as the intersection of the black circles). (**G**) Precision of the localization system (*27*), showing localization error of σ = 8.9 cm along the tunnel's major axis. (**H**) Example session, showing the *y*-*z* positions of the bat's passages (blue dots) through a cross-section in the tunnel's midpoint (black outline). There are relatively small deviations of the blue dots in the *y* and *z* axes, indicating the bat flew essentially in 1D trajectories (fig. S3, B and C). (**I**) Example session showing speed profiles along the tunnel, pooled over both flight directions. Gray areas indicate locations of low flight speeds, owing to takeoff and landing, which were removed from further analysis of place fields (*27*). (**J**) Distribution of the coefficient of variation (CV) of the flight speed per session (n = 60 sessions; five bats). The CV was computed over the tunnel's high-speed portion [excluding the gray areas from (I)]; mean CV = 0.042. (**K**) Distribution of number of flights (laps) per direction per session. Shown are only valid unidirectional long flights, longer than 100 m (*27*). Red and blue colors in (K) and (J) indicate the two flight directions (arrows). (**L**) Distribution of total distance flown per session, based on valid long flights only (n = 60 sessions; five bats).

in our 200-m environment. First, unlike the typical single place field reported for CA1 neurons in small environments (*11*), we found that many cells exhibited multiple place fields (Fig. 2A and fig. S5, examples; Fig. 2G, population). The mean number of fields per direction was 4.9, and some neurons had more than 10 fields in each flight direction (Fig. 2G). This result extends similar findings in enlarged environments in rodents, which showed several fields per neuron (*18*, *31*, *32*). The fields were strongly tuned and contained the large majority of the neuron's spikes; the background firing was relatively low (fig. S6, A and B). Second, many cells had very large place fields, often >10 m in size, and up to 32 m (Fig. 2, A, cells 1 and 5, examples, and H, population; and figs. S5 and S7A). On the other hand, some cells had very small place fields of <1 m in size and down to 0.6 m (Fig. 2, A, cells 3 and 7, zoom-in, and H, leftmost bar). The distribution of field sizes was skewed (Fig. 2H) and was well-fitted by a log-normal distribution (fig. S8) (*33*). Third, and most surprisingly, many place cells showed highly variable field sizes, with up to 20-fold ratio between the size of the largest and smallest field for the same neuron (Fig. 2A, cells 1 to 7, examples; and Fig. 2, I and J, population; mean ratio, 4.4). This multifield, multiscale code was found

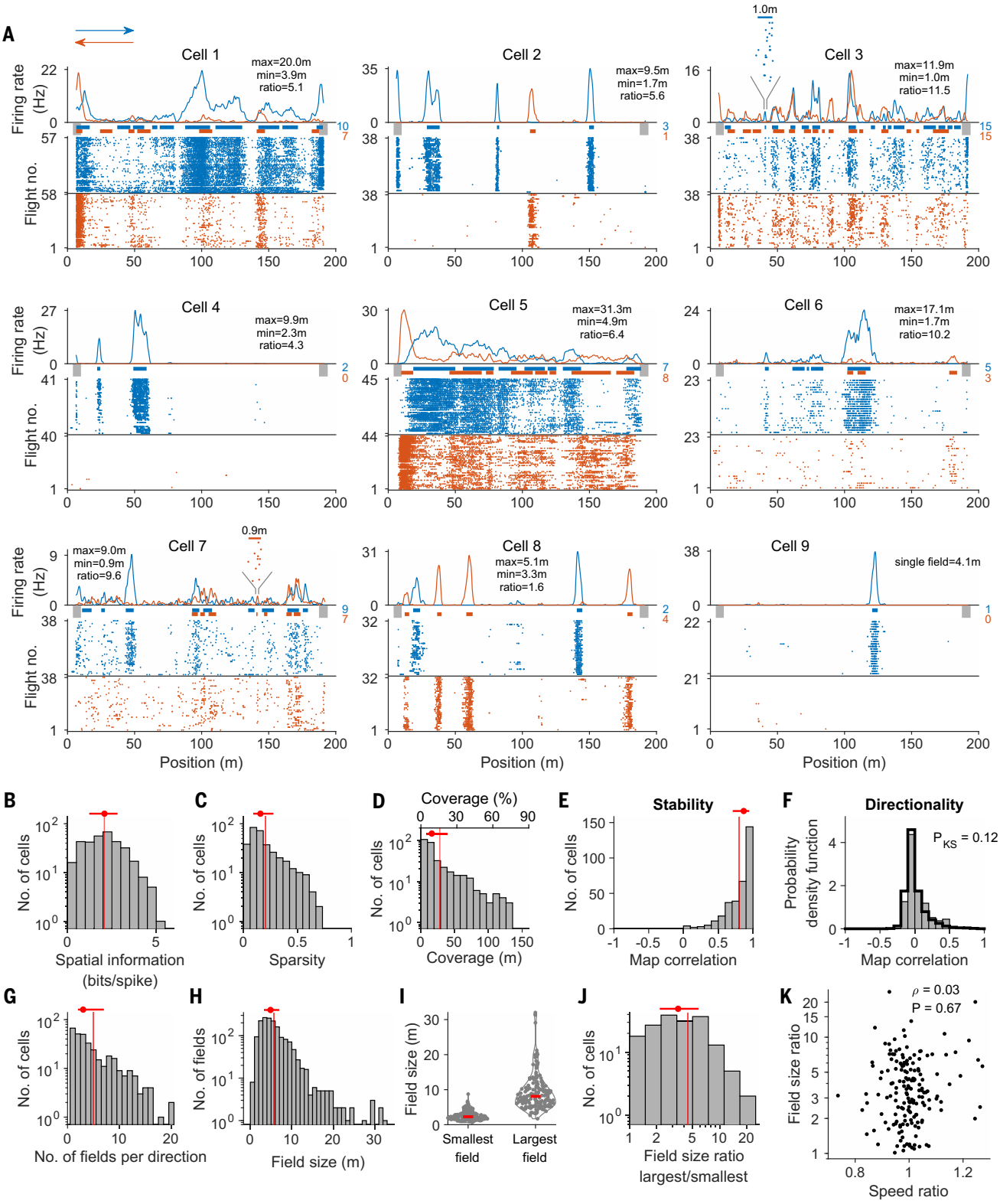

Fig. 2. Dorsal CA1 hippocampal neurons represented very large space using many fields with multiscale coding. (**A**) Examples of firing-rate maps and raster plots for nine cells. For each neuron, (Top) firing-rate maps calculated separately for each flight direction (red and blue; arrows above cell 1); (Bottom), raster plots of spike positions (*x* axis) for different flights, or laps (*y* axis); the detected place-fields are indicated with red and blue thick horizontal lines above the raster plots [fields inside the low-flight-speed zones (gray) were excluded (*27*)]. In each example, the smallest and largest field sizes are indicated (min, max), together with the ratio between them; the numbers of fields in each direction are indicated in blue and red on the right. For cells 3 and 7, shown also are zoom-ins on their smallest field (cell 3, field size 1.0 m; cell 7, field size 0.9 m). (**B** to **D**) Distribution of (B) spatial information, (C) sparsity, and (D) the total coverage of the environment by place fields, calculated for the firing-rate map in each flight direction separately ("No. of cells" here refers to significant

cells × directions; n = 331). (D) Bottom x axis, total coverage in meters; top x axis, total coverage in percent of tunnel length. (**E**) Distribution of firing-map correlations between odd and even flights (n = 331 cells × directions), showing high correlation values [median correlation coefficient (r) = 0.87]. (**F**) Distribution of firing-map correlations between the two flight directions (gray; n = 135 cells, including only cells where both directions were significantly tuned) was similar to cell-shuffled distribution (black) [Kolmogorov-Smirnov test: P = 0.12 ($D_{KS\ 135,13566}$ = 0.10)]. (**G**) Distribution of number of place fields per neuron per flight direction (n = 331 cells × directions). Rightmost bar, cases with ≥20 fields per direction. Mean number of fields per direction was 4.9. (**H**) Distribution of place field size (n = 1629 fields). The field size ranged from <1 m (leftmost bar of histogram) up to 32 m. (**I** and **J**) Single cells exhibited multiscale field sizes (plotted are n = 172 cells with ≥2 fields). (I) Distributions of smallest and largest field sizes per neuron (shown cells with ≥2 fields). (J) Distribution of the ratio between largest and smallest field sizes for each neuron. Both axes here are in log scale. (**K**) Lack of correlation between largest-to-smallest field size ratio and the speed ratio at the locations of those fields (plotted are n = 172 cells with ≥2 fields). For all histograms except (F), the red vertical line indicates mean of distribution, and the red dot and red horizontal line indicate median and interquartile range, respectively.

in all the five individual animals (fig. S9). Although most cells showed heterogeneous field sizes, some neurons also exhibited a more uniform scale across their place fields (Fig. 2A, cell 8), and a small minority of neurons had a single place field (Fig. 2A, cell 9) (only 12.2% of the neurons had one field overall, with an average field size of 5.9 ± 3.5 m; mean ± SD). Individual neurons exhibited similar multiscale firing properties in both flight directions: a similar number of fields per direction, similar median field-size, and similar field size ratios (fig. S10). This suggests a characteristic firing propensity per neuron (*34*) while still exhibiting widely varying field sizes. Taken together, most neurons exhibited these two key properties: many fields per neuron (Fig. 2G) and a multiscale mixture of small fields and large fields for the same neuron (Fig. 2J).

We next examined several possible alternative explanations for the multiscale code that we observed. First, the multiscale property could not be explained as arising from variations in flight-speed—for example, larger fields at high flight speeds—because the flight speed was in fact highly consistent along the entire tunnel (Fig. 1, I and J). Further, the field-size ratio (largest/smallest fields per neuron) was not correlated with the speed ratio at the locations of the largest and smallest fields (Spearman ρ = 0.03, df = 170, P = 0.67) (Fig. 2K). Moreover, the speed ratio was narrowly distributed around 1, indicating that the speed was similar at large and small fields (Student's t test of speed ratio versus 1: t = 0.83, df = 171, P = 0.41; SD of the speed ratio was 0.10) (Fig. 2K). Second, the multiscale property also could not be explained by systematic differences in field sizes in the long versus short arms of the tunnel because we found no significant difference in field sizes between the two arms [Kolmogorov-Smirnov test comparing field sizes in the long versus short arm: P = 0.60 and 0.12 for the two flight-directions ($D_{KS\ 586,180}$ = 0.06 and $D_{KS\ 628,235}$ = 0.09)], and there was no significant difference in field sizes between the long arm and the full tunnel [Kolmogorov-Smirnov test: P = 0.96 ($D_{KS\ 1214,1629}$ = 0.02)] (fig. S7A). We also found multiscale coding when restricting the analysis only to the long arm (fig. S7B). Third, the multiscale property did not stem from an unusual recording location within CA1. All the recordings were done in the dorsal part of the hippocampus and spanned rather central proximo-distal locations in CA1 (fig. S1, A and B); these are the classical recording-locations used in rodents and bats in small laboratory setups. Fourth, the multiscale property of CA1 neurons could not be explained by spike-sorting quality (fig. S11). Fifth, the results were robust to the detailed criteria of field detection (fig. S12).

We then looked for possible contributions of landmarks to the multiscale code. First, we considered several landmark-based compartmentalization models of the environment, in which the tunnel is assumed to be segmented into smaller portions at the landmark locations, allowing fields to merge at the segment borders (*27*). These models could not explain the wide distribution of place field sizes observed in the data (fig. S13). Second, we examined the possibility that the multiscale code could be explained by an overrepresentation (concentration) of place fields near the landmarks, and in particular small place fields. However, the cumulative distribution of field locations was linear as a function of position along the tunnel (Fig. 3A), with no apparent overrepresentation near landmarks [but with an overrepresentation of fields at the two ends of the tunnel, in the reward areas (fig. S14)]. We computed the distance of each field's peak to its nearest landmark and compared the distribution of these distances to the distribution of distances for shuffled place field locations (*27*); we found no significant difference between the two (Kolmogorov-Smirnov test, $P \geq 0.18$ for both directions) (Fig. 3B), indicating that place fields did not concentrate near landmarks but were distributed rather uniformly along the tunnel. This uniform distribution was supported also by an analysis of the gaps between fields, which showed an exponential distribution (Fig. 3C), indicating lack of structure in the spatial arrangement of place fields. Additionally, the entire range of field sizes was represented rather uniformly along the tunnel, with no prominent concentration of small (or large) fields near landmarks (Fig. 3, D and E, and fig. S15)—likely because of the low saliency of these landmarks for the bats—except for a few landmarks that possibly showed slight concentration of fields (Fig. 3D). Further, there was no strong relation between the interlandmark distance and the field size (fig. S15B) (however, this does not rule out that very large fields would be found in extremely impoverished large regions of space, where absolute spatial information is not available over long distances). Together, these analyses suggest that the multiscale statistics were not driven by landmarks.

Comparison between large and small environments

To examine whether multiscale coding may be found also in small environments, we recorded from the dorsal CA1 of an additional three bats flying in a short 6-m segment of the tunnel, which we blocked off (table S1, dataset 2) (Fig. 4A). This allowed testing directly the effect of environment size on the spatial coding of neurons in the dorsal CA1 of bats, using the same experimental design. The percentage of neurons that were active during flight in the short 6-m tunnel (36 of 67 cells, 53.7%) was much smaller than in the full 200-m tunnel (235 of 235 cells, 100%) (table S1) (*27*). The majority of the active cells were significant place cells (30 of 36, 83.3%); thus, almost half of the neurons recorded in the 6-m tunnel were significant place cells (30 of 67 cells, 44.8%). Next, we systematically compared the spatial tuning properties of cells in the large versus small environments (Fig. 4, B to G). In the 6-m small environment, dorsal CA1 place cells showed only one or two place fields (Fig. 4, A and B, bottom), in contrast to the high number of place fields observed in the large 200-m environment (Fig. 4, B, top, and E). Across cells, the place field sizes in the small environment were much smaller than in the large environment (Fig. 4, C and F). At the single-cell level, neurons in the small environment had a significantly lower ratio between their largest and smallest fields as compared with that in the large environment (Fig. 4, D and G). Thus, neurons in the small environment showed virtually no multiscale coding.

Multiscale coding of space is independent of both early and recent experience

Does multiscale coding of large environments emerge over time, as a function of experience? First, we asked whether prior experience in the long tunnel is needed for the multiscale code. We conducted recordings of place cells

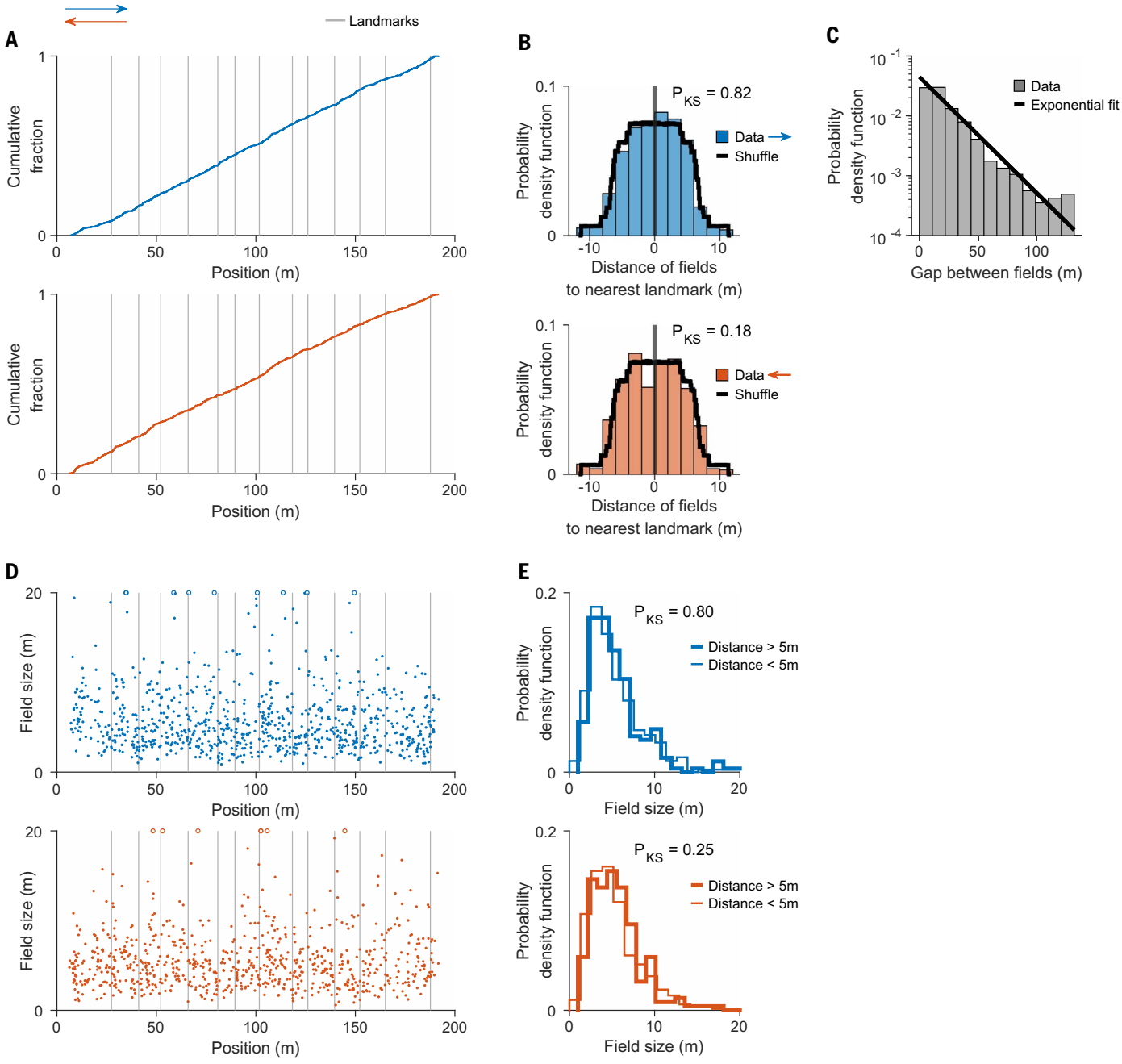

Fig. 3. Place fields were distributed uniformly along the tunnel. (**A**) Cumulative fraction of peak firing-rate locations for all the place fields along the tunnel, pooled across all the five bats and 196 place cells; plotted for each flight-direction separately (East direction, blue, n = 863 fields; West direction, red, n = 766 fields). Gray vertical lines, locations of landmarks (we did not treat the landing balls as "landmarks"). (**B**) Distributions of the distances of each field's peak to its nearest landmark (blue and red, flight directions) were similar to shuffle distributions (black) [Kolmogorov Smirnov test, P = 0.82 ($D_{KS\ 782,7820000}$ = 0.02) and P = 0.18 ($D_{KS\ 661,6610000}$ = 0.04) for the two flight directions]. (**C**) Distribution of gaps between fields (gray bars), overlaid with exponential fit (black line), plotted on a logarithmic y scale. The good fit to the exponential distribution indicates lack of spatial structure in the field locations. (**D**) Field size versus the location of field peak, pooled across all bats and neurons. Gray vertical lines, locations of landmarks; open circles, fields larger than 20 m. The entire range of field sizes was represented along the entire tunnel. (**E**) Distribution of field size for the two directions (blue and red), plotted separately for fields located close to landmarks (thin line, fields <5 m from nearest landmark) or far from landmarks (thick line, fields ≥ 5 m from nearest landmark). No significant differences in field-size were found between fields located close or far from a landmark [Kolmogorov Smirnov test, P = 0.80 ($D_{KS\ 577,205}$ = 0.05) and P = 0.25 ($D_{KS\ 469,192}$ = 0.09) for the two flight directions]. In (B) and (E) we excluded fields whose peak occurred before the first landmark or after the last landmark in the tunnel, where the assignment of "nearest landmark" is one-sided and hence biased [the same was done for the shuffles in (B)].

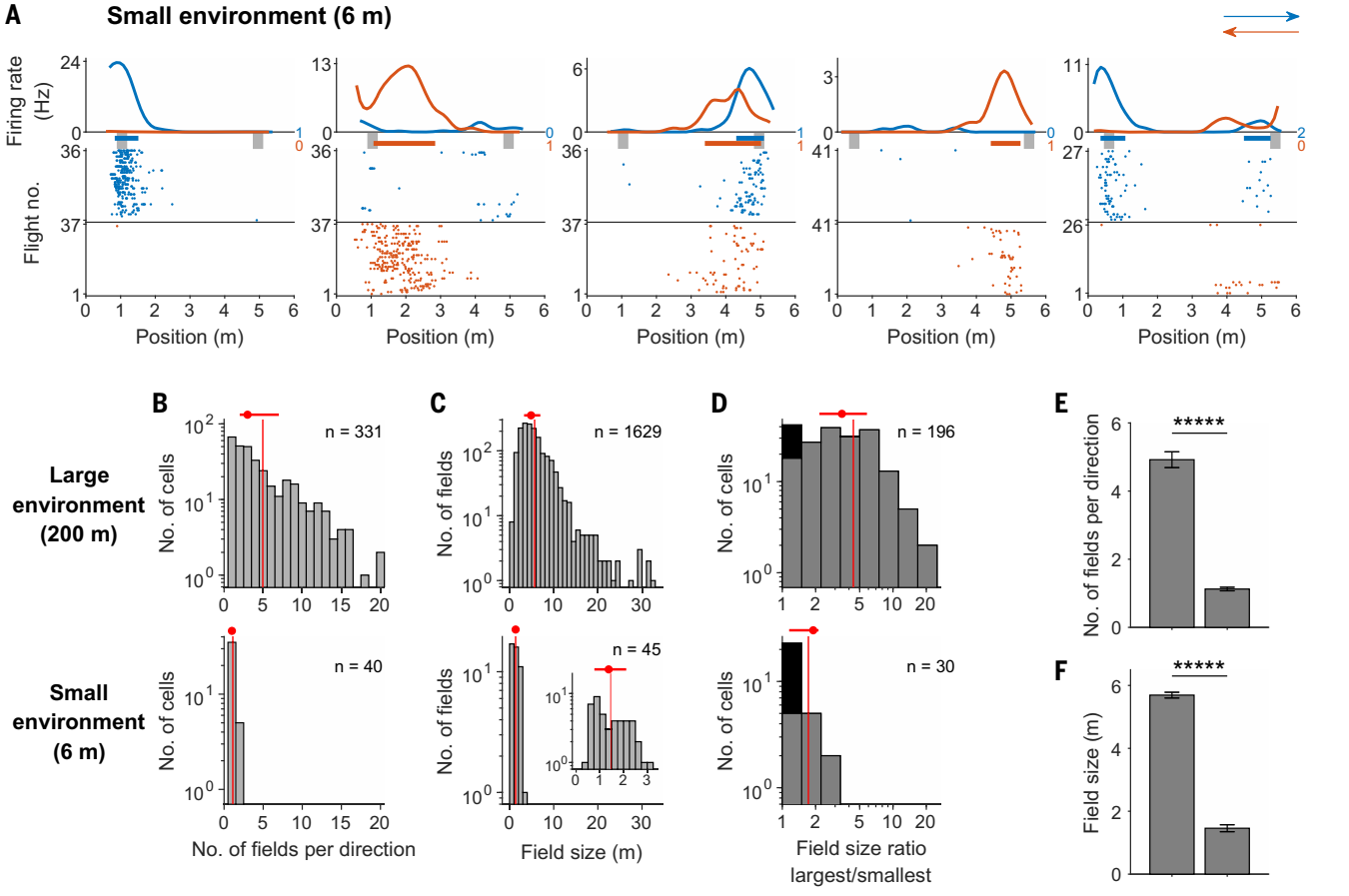

Fig. 4. No multiscale coding was found in a small-scale environment. Experiments were done in a small 6-m segment of the long 200-m tunnel, which we blocked with two curtains (table S1, dataset 2). (**A**) Examples of firing-rate maps and raster plots for dorsal CA1 place cells recorded in this small-scale environment. Same graphical conventions as in Fig. 2A. Most cells had a single field per direction, or two fields with a similar scale. (**B** to **D**) Distributions of (B) number of fields, (C) field sizes, and (D) field size ratio for the two different dorsal CA1 datasets: large-scale 200 m environment (top row) and small-scale 6 m environment (bottom row). Red vertical lines, mean of distribution; red horizontal lines and red dot, interquartile range and median, respectively. (C) (Inset) Zoom-in. Black bars in (D) show neurons with one field. (**E** to **G**) Comparison between the two datasets (large versus small environment), for the three quantities: (E) number of fields, (F) field sizes, and (G) field size ratio (here, we included only neurons with ≥2 fields). Error bars, mean ± SEM. There was a highly significant difference in all of these three quantities between large-scale and small-scale environments, indicating that the multifield, multiscale coding is expressed most prominently in large-scale environments. (E) Student's *t* test with unequal variances, $P = 6.7 \times 10^{-44}$, $t = 15.94$; Wilcoxon rank-sum test, $P = 1.5 \times 10^{-15}$, $z = 7.89$. (F) Student's *t* test with unequal variances, $P = 4.5 \times 10^{-58}$, $t = 29.56$; Wilcoxon rank-sum test, $P = 3.9 \times 10^{-26}$, $z = 10.51$. (G) Student's *t* test with unequal variances, $P = 1.8 \times 10^{-14}$, $t = 8.91$; Wilcoxon rank-sum test, $P = 4.6 \times 10^{-5}$, $z = 3.91$; ***** $P < 10^{-5}$ for the *t* tests in (E) to (G).

from the first exposure to the novel large environment. We recorded 125 place cells from two bats flying in a 130-m portion that was blocked out of the 200-m tunnel, with neural recordings commencing from the very first day in the tunnel (day 1) and continuing over several weeks (with new cells being recorded every day) (table S1, dataset 3). Cells were spatially tuned already in the first sessions and exhibited many place fields with different sizes (Fig. 5A). The multifield, multiscale properties were seen from day 1 and were stable across several weeks of recordings, showing no significant trend in the number of fields (Fig. 5B), field sizes (Fig. 5C), or field-size ratio (Fig. 5D) [overall, place fields in the 130-m tunnel exhibited somewhat smaller numbers of fields, field sizes, and field-size ratios as compared with those of the 200-m tunnel (Fig. 5, B to D, bars on the right)]. This suggests that the multiscale coding does not require substantial recent experience with the long tunnel. Although the general multiscale properties were stable over days (Fig. 5, B to D), the cells occasionally exhibited within-day dynamics in the form of fields appearing and disappearing (Fig. 5E). The rate of within-day changes was larger during the first 2 days of the bat in the tunnel (two-proportion *z* test, $P < 0.001$) (Fig. 5F) but also occurred many days after the first exposure (Fig. 5, E, cells 7 and 8, and F), which is consistent with previous findings in mice of ongoing changes in the tuning of place cells (*35*, *36*).

Second, we asked whether laboratory-born bats that were never exposed to large environments would lack a multiscale code. We recorded from an additional three adult bats that were born in the laboratory and grew up in an enriched environment but had never experienced during development any large-scale environments bigger than a few meters (table S1, dataset 4, and fig. S16) (*27*)—in contrast to the wild-caught bats that navigated long distances outdoors during development (*37*). The laboratory-born bats were trained to fly in the 200-m tunnel for several weeks and were thus familiar with the environment before the

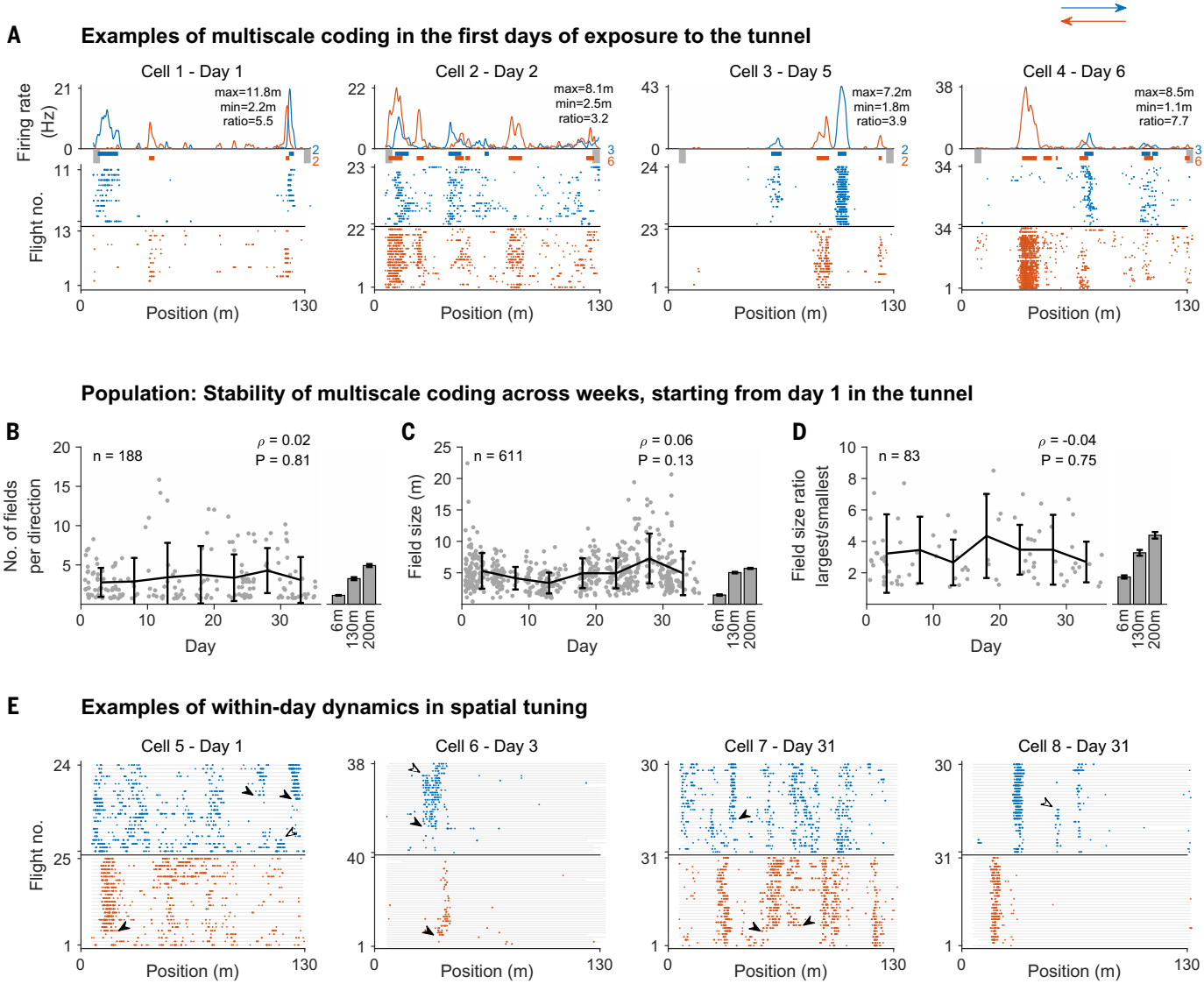

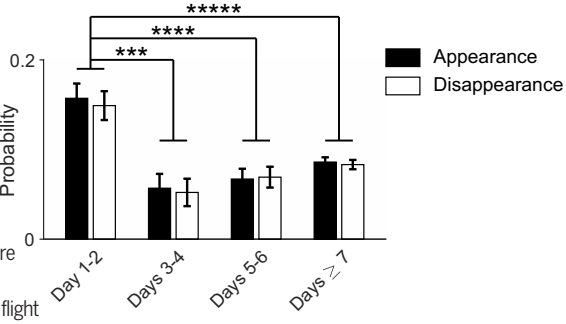

Fig. 5. Multiscale coding exists already from the first days of exposure to the tunnel. Experiments from day 1 were conducted in a 130-m portion of the 200-m tunnel (table S1, dataset 3). (**A**) Examples of firing-rate maps and raster plots for four cells recorded in a large-scale environment during the first days of exposure. Same graphical conventions as in Fig. 2A. The days since first exposure are indicated for each cell (day 1 is the very first day of exposure; day count represents experimental days). (**B** to **D**) Population scatter plots of (B) the number of fields per direction, (C) field sizes, and (D) field size ratio as a function of days since first exposure. There is a lack of trend across days (Spearman ρ, $P > 0.13$ for all three scatters), suggesting that the multiscale coding exists already from day 1. For display purposes only, dots were jittered along the *x* axis (uniform jitter of ±0.5 days); in (B), dots were jittered also along the *y* axis (uniform jitter of ±0.3 fields); all correlations were computed without the jitter. Error bars in main plots, mean ± SD (using 5-day bins with no overlap). (Insets) Gray bars are mean ± SEM for the three tunnel lengths used in this study: 6, 130, and 200 m. (**E**) Four examples of within-day dynamics in spatial tuning. Raster plots show spike positions in each flight (blue and red dots indicate two flight directions), with the behavioral coverage shown with light gray lines. Arrowheads indicate field appearance (filled arrowheads) or disappearance (empty arrowheads). These dynamics occurred in both small and large fields and happened both on the first days of exposure (cells 5 and 6) and after ≥1 month (cells 7 and 8). (**F**) Probability of appearance and disappearance of fields (per-flight probability of change in any of the fields), grouped by the day from first exposure: days 1 and 2, days 3 and 4, days 5 and 6, and ≥7 days. Error bars, mean ± standard error of the proportion (*27*). In the first 2 days after exposure, the cells exhibited a higher probability of appearance or disappearance of fields than on later days (two-proportion *z* test, $P < 0.001$ for all six tests comparing days 1 and 2 versus the other days). The probabilities for appearance and disappearance were similar over the entire course of exposure (compare black versus white bars; two-proportion *z* test: $P = 0.64$, pooled over all days), which is consistent with the overall stability over weeks in the number of fields per neuron (B). *****$P < 10^{-5}$, ****$P < 10^{-4}$, ***$P < 10^{-3}$.

neural recordings, similar to the wild-born bats (Fig. 6A). The laboratory-born bats were in good flight shape and flew similar distances in the tunnel as those of the wild-born bats (fig. S16B). Thus, the main difference between the laboratory-born and wild-born bats was their experience during development, with all other experimental conditions being kept identical (Fig. 6A) (*27*). We recorded 113 cells in the dorsal CA1 of the laboratory-born bats, out of which 95 were place cells (84.1%), which is very similar to the percentage of place cells in wild-born bats (83.4%). The place cells of laboratory-born bats showed a multifield, multiscale code, with individual neurons exhibiting many fields with varying sizes per-neuron (Fig. 6B, examples; Fig. 6, C to E, population), which is similar to place cells recorded from the wild-born bats. We then compared the multiscale properties between the two groups (Fig. 6, C to H): (i) The number of fields per direction was not significantly different (Fig. 6, C and F). (ii) Both groups exhibited wide distributions of place field sizes, with wild-born bats having slightly larger fields (Fig. 6, D and G) [this difference was not due to differences in dorso-ventral recording positions along the longitudinal axis of CA1, which were very similar in both groups (Fig. 6I), but could be due to the slightly different recording positions along the proximo-distal axis of CA1 (Fig. 6I)]. (iii) The field-size ratio was not significantly different between the groups (Fig. 6, E and H), despite the difference in field sizes—indicating a similar multiscale code between laboratory-born and wild-born bats.

The multiscale code yields substantial advantages for large environments

We next turned to a theoretical analysis to understand the possible functional advantage of the multiscale representation of large environments. We compared the performance of six spatial encoding schemes (Fig. 7A) (*27*): (scheme 1) a single small place field per neuron; (scheme 2) a single large place field per neuron; (scheme 3) a single place field with a gradual increase in field size across the population, mimicking the dorso-ventral anatomical gradient of field sizes in the hippocampus (*17*); (scheme 4) multiple small fields per neuron, identical in size for all the neurons (*18*); (scheme 5) multiple fields per neuron, all with the same size for each neuron but with different scales across different neurons; and (scheme 6) multiple fields with multiscale coding per neuron, as in our data. The distribution of field sizes for schemes 5 and 6 was matched to our data [field sizes were drawn from a γ-distribution fitted to the data (fig. S8) (*27*); the field-size ratio for scheme 6 also closely matched the data (fig. S17G); variants of schemes 5 and 6 in which we matched also the total coverage of fields to the data are shown in fig. S17]. We used two types of decoders, a Bayesian maximum-likelihood decoder (Fig. 7) and a population-vector decoder (fig. S18), and two integration time windows, Δt = 500 ms (Fig. 7) and Δt = 200 ms (fig. S19) (*27*). We compared the decoding error of simulated data for each of these six encoding schemes for progressively larger environments. For small environments, all six encoding schemes performed qualitatively equally well, but for very large environments (hundreds of meters), the experimentally observed encoding scheme with multiscale place fields substantially outperformed the other schemes (Fig. 7, B to E, and fig. S18, B to E). Specifically, for encoding schemes with either a single field (schemes 1, 2, or 3) or multiple fields of small size (scheme 4), the number of neurons required to accurately decode the animal's position was extremely large for large environments (Fig. 7B, left; the red, green, pink, and yellow lines go out of bounds). By contrast, the two schemes with multiple fields of varying sizes (schemes 5 and 6) required only ~50 neurons for accurately decoding the bat's position, even in a very large environment of 1000 m in size (Fig. 7B, left; a 2-m decoding accuracy). Furthermore, the mean decoding error for schemes 1 and 4 increased dramatically for large environments (Fig. 7C, red and green), but for schemes 5 and 6, the mean decoding error barely increased as a function of the environment size (Fig. 7C, inset, blue and purple), maintaining a small decoding error of 5 to 10 m for a 1000-m environment, even for a very small ensemble of 50 neurons (Fig. 7C, inset). We thus conclude that encoding schemes 1 to 4 are less suitable for very large environments.

Next, we asked whether scheme 6, which closely matches our experimental results, offers any functional advantage over scheme 5. We reasoned that scheme 5, in which all the fields of the same neuron have the same field size, is problematic because when a neuron emits a spike, it could mean that the animal is located in any of the neuron's fields; this creates large positional ambiguity. By contrast, scheme 6, in which each neuron has multiscale fields, alleviates this problem because the neuron's spike count during an integration time Δt differs between different fields—the neuron produces many spikes in large fields but only a few spikes in small fields—and this variability serves to disambiguate which field the animal passed through; this in turn improves the decoding accuracy. For large, 1000-m environments, the mean decoding error was substantially smaller for scheme 6 than for scheme 5 (Fig. 7C, inset, compare purple and blue lines). Moreover, scheme 6 led to much smaller and fewer catastrophic decoding errors (Fig. 7, D and E, compare purple and blue lines) [There is a ~10-fold difference in the size of catastrophic decoding errors, defined as the 99th percentile of the decoding errors (Fig. 7D, inset) and an approximately two- or threefold difference in the probability of catastrophic errors, which is defined as the probability of decoding error larger than 5% of the environment size (Fig. 7E)]. All of these theoretical results were robust to the choice of decoder type (fig. S18), the choice of integration time window of the decoder (fig. S19), and choice of the parameter that controls the scaling of encoding schemes with environment size (fig. S17H) (*27*). Together, this theoretical analysis suggested that for small environments, all the encoding schemes perform equally well (Fig. 7, B to E; all six lines meet at the environment size of 20 m); by contrast, for very large environments, of hundreds of meters or more, scheme 6—which matches the multiscale coding that we found in bat CA1—outperforms all the other coding schemes.

Last, we suggest that the absence of a multiscale code in small environments might stem from energy considerations. We used published experimental estimates of the energy [adenosine triphosphate (ATP) molecules] required to generate one action potential (*27*, *38*) to approximate the energy required to represent environments of different sizes for the various coding schemes (Fig. 7F). In small environments, classical single-field codes (schemes 1 to 3) were more energetically efficient than our multiscale code (scheme 6). Because all of the codes exhibit a similar localization performance in small environments, the energetic consideration becomes more important, and therefore the single-field codes are preferable for small environments. By contrast, in large environments our multiscale code becomes energetically closer to the single-field codes and even surpasses some of them in terms of energy consumption (Fig. 7F, compare scheme 6 with the other schemes). Further, the localization accuracy of classical single-field codes deteriorates so greatly in large environments (Fig. 7, C to E) that the energetic consideration becomes largely irrelevant, and the superior localization accuracy of the multiscale code becomes the central consideration. Thus, we propose that this energetic consideration—and in particular, the tradeoff between energy expenditure and coding performance—may explain why in small environments there is no multiscale code. Taken together, the theoretical decoding analyses suggest that the multiscale code is better suited than classical place codes for representing very large spaces, such as real-world natural environments.

Neural network modeling of multiscale codes: Attractor networks and feedforward models

Classical models of hippocampal place cells are characterized by a single spatial scale per neuron in a given environment (*39*–*47*). We investigated two types of models that might support multiscale representations (figs. S20

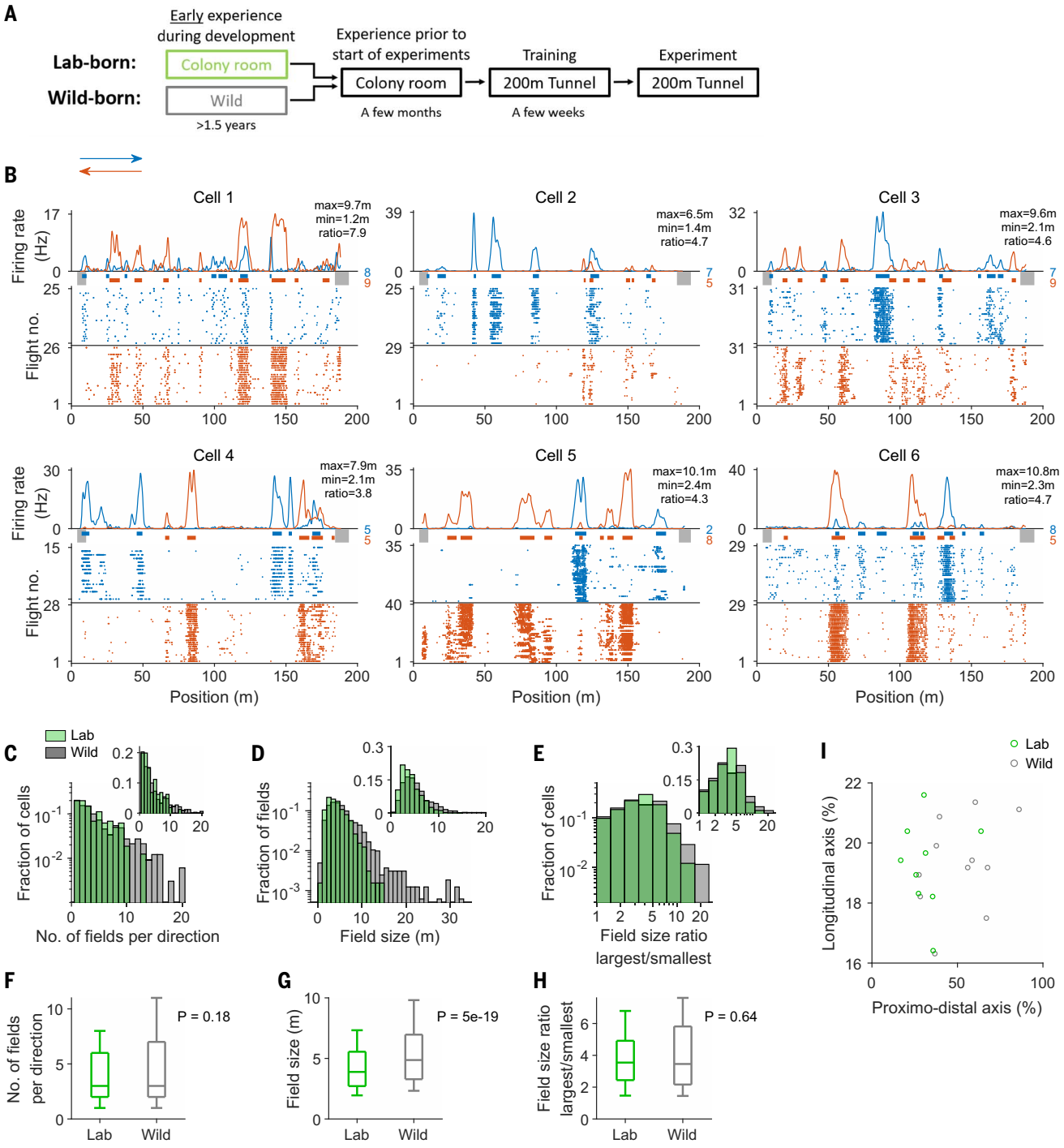

Fig. 6. Multiscale coding does not require early exposure to large-scale environments during development. Comparison of multiscale properties between laboratory-born bats that were raised in a 5-m-sized room (*27*) and have never experienced large-scale environments during development (green) (table S1, dataset 4) versus wild-born bats that were caught as adults outdoors (gray). Both groups of bats were tested under identical conditions in the 200-m tunnel. (**A**) Schematic of experimental design. The only difference between laboratory-born and wild-born bats occurred during early life; subsequent stages were identical: Both groups spent several months in the same colony-room before surgery, and then the training and recording procedures were identical for both groups. (**B**) Examples of firing-rate maps and raster plots for six cells recorded from laboratory-born bats flying in the large-scale environment (200-m tunnel). Same graphical conventions as in Fig. 2A. (**C** to **E**) Distributions of (C) number of fields per direction, (D) field sizes and (E) field-size ratio for laboratory-born bats (green) and wild-born bats (gray), recorded in the same large-scale environment. (C) n_{lab} = 161 cells × directions, n_{wild} = 331. (D) n_{lab} = 649 fields, n_{wild} = 1629. (E) n_{lab} = 82 cells, n_{wild} = 172 [only cells with ≥2 fields shown in (E)]. *y* axes are in log scale. (Insets) Same histograms with *y* axis in linear scale. (**F** to **H**) Population comparisons between laboratory-born and wild-born bats: (F) number of fields per direction, (G) field sizes, and (H) field-size ratio. Boxplots denote the median (horizontal line), 25 to 75% (box), and 10 to 90% (whiskers); *P* values of Wilcoxon rank-sum tests are indicated. (F) *df* = 490, *z* = −1.33. (G) *df* = 2276, *z* = −8.92. (H) *df* = 252, *z* = −0.47. Despite significant difference in the

field-sizes distribution [(G) $P = 5 \times 10^{-19}$], the field-size ratio distribution did not differ significantly [(H) $P = 0.64$], indicating that the multiscale code exists also in neurons recorded from laboratory-born bats. (**I**) Anatomical positions of tetrodes along the CA1 longitudinal (dorso-ventral) axis and proximo-distal axis [0% longitudinal: dorsal (septal) pole of CA1; 0% proximo-distal, proximal border with CA2]. Tetrodes from both groups had similar longitudinal coordinates in dorsal CA1, but laboratory-born bats' tetrodes concentrated more proximally along the proximo-distal axis of CA1.

to S23 and supplementary text). First, we used a continuous attractor neural-network framework (fig. S20, A to C) (*40*, *42*–*44*, *47*, *48*). We generated a network with multiple interacting attractors at various scales, in which each neuron could participate in any of the attractors at a random location (fig. S20A) (*27*). Network simulations showed coherent bumps of activity at each attractor, with different bump widths (fig. S21, A and B), and single neurons exhibited multifield, multiscale coding (fig. S20B) that was consistent with our experimental data. Second, we explored a set of feedforward models, in which CA1 neurons received inputs from CA3 and medial entorhinal cortex (MEC) with diverse synaptic strengths (fig. S20, D to J) (*27*). The modeling suggested that the experimental data were inconsistent with a strong periodic grid input and were most consistent with a model in which the major input into CA1 comes from CA3, in which individual CA3 neurons exhibit a single place-field (supplementary text and fig. S20J). We thus predict that in very large environments, (i) MEC neurons should not exhibit strong periodicity, and (ii) place cells in CA3 (unlike those in CA1) should exhibit single place fields.

Discussion

We found a multiscale neural code for large environments: Single hippocampal neurons in the dorsal CA1 area of bats exhibited many fields, and the different fields of the same neuron varied dramatically in size, with an up to 20-fold ratio in the size of different place fields for the same neuron. This unknown coding scheme was revealed through the use of an extremely large environment. This finding constitutes a fundamentally different phenomenon from the well-known gradient of place field sizes along the longitudinal anatomical axis of the hippocampus (*14*, *17*, *49*)—where each neuron has one characteristic spatial scale, and this scale changes between neurons according to anatomical position. In this study, by contrast, all the recordings were conducted in the same anatomical position, the dorsal CA1 (fig. S1), and we found that individual neurons did not have a single scale but rather that the spatial scale of the same neuron varied dramatically across the environment. Further, this neural code was observed from the first day of exposure to the environment and was similar between laboratory-born and wild-born bats, suggesting that the multiscale code is a very robust phenomenon that does not require substantial recent experience with the test environment nor early experience with large environments in general.

Previous studies in rodents have reported multiple place fields for individual CA1 neurons in (relatively) large environments (*18*, *31*, *32*)—although the number of fields per neuron was much smaller than we found here—but no study to date has found the multiscale property that we discovered here for individual neurons. Our theoretical decoding analysis provides a simple functional explanation for this multiscale code: For very large environments, multiscale coding outperforms all the other codes that we considered, in terms of reducing the number of required neurons and minimizing the decoding errors. We hypothesize that the reason why previous studies (*18*, *31*, *32*) did not find a multiscale code was that they used much smaller environments, or concatenated small compartments, where such a code does not provide a functional advantage. Recordings from bats flying in a small environment did not show a multiscale code (Fig. 4).

The absence of a multiscale code in the small environment can be interpreted in two ways: (i) Neurons in small environments exhibit the classical place code and switch to a multiscale code in large environments. (ii) Multiscale coding is the underlying representation in all environmental scales, but the multiscale nature of the code cannot be revealed in small environments, where the firing reflects a small "pinhole view" of the larger multiscale map, and therefore the largest fields are too big to be seen because they cover the entire space. However, option (ii) seems unlikely because we would then expect to see in the 6-m setup many neurons that fire over the entire environment, thus reducing substantially the percentage of place cells out of the neurons active in flight—but in fact, these percentages were remarkably similar between the 6-m and 200-m environments (83.3 and 83.4%, respectively).

Our multiscale findings open the way for numerous future questions on the neurobiology of large-scale navigation. For example: What are the mechanisms that underlie this multiscale coding that we discovered? Our network modeling suggested that one possibility is a feedforward convergence of inputs from CA3, where each CA3 neuron has a single field (fig. S20, D, left, and J), and also predicted that MEC neurons should not exhibit spatial periodicity in large environments (fig. S20, G to I). Further, what is the biological decoder that may read this code downstream? How are such large spaces learned by the hippocampal system? Are there ultralong compressed firing sequences during rest and sleep, similar to sequences observed in laboratory environments (*50*–*52*), but extending over hundreds of meters or more? If so, what are the mechanisms that could create these sequences under this multiscale code, in which each neuron would participate multiple times in each sequence, each time with a different resolution? More broadly, these findings call for performing neurophysiological research in very-large-scale environments on all types of hippocampal and entorhinal spatial neurons. We posit that such research is crucial for understanding the brain's "navigation circuit" for two reasons: First, most animals and humans evolved to navigate in multicompartment environments with different spatial scales, including very large scales, so it is important to conduct neurobiological research on large scales. Second, studies in humans have emphasized that spatial scale is important for navigation; people navigate differently in large versus small environments, which calls for conducting navigation experiments in very large environments (*53*). Our study provides direct single-neuron evidence that the use of a real-world spatial scale can reveal a fundamentally new kind of spatial coding in the hippocampus. This work thus makes a step toward bridging the major gap between the neurobiological tradition of studying the brain's navigation circuit in small-scale laboratory setups and the ecological tradition of studying large-scale animal navigation outdoors.

Materials and methods summary

We conducted tetrode-based recordings of single neurons in the dorsal hippocampus area CA1 of Egyptian fruit bats (*Rousettus aegyptiacus*), in both wild-born and laboratory-born bats, using a wireless electrophysiology system, while the bats were flying in a very large environment (200-m-long tunnel), in either familiar or novel conditions. For comparison, we also recorded from bats flying in a 6-m segment of the tunnel. The experimental datasets are summarized in table S1. We localized the bat's position in the tunnel using a radio frequency–based system yielding ~9-cm precision. We computed firing-rate maps separately for each flight direction and used spatial information and a shuffling procedure to identify significant place cells. Individual place fields were detected as prominent, stable, and significantly tuned peaks in the firing-rate maps. To theoretically compare the observed spatial

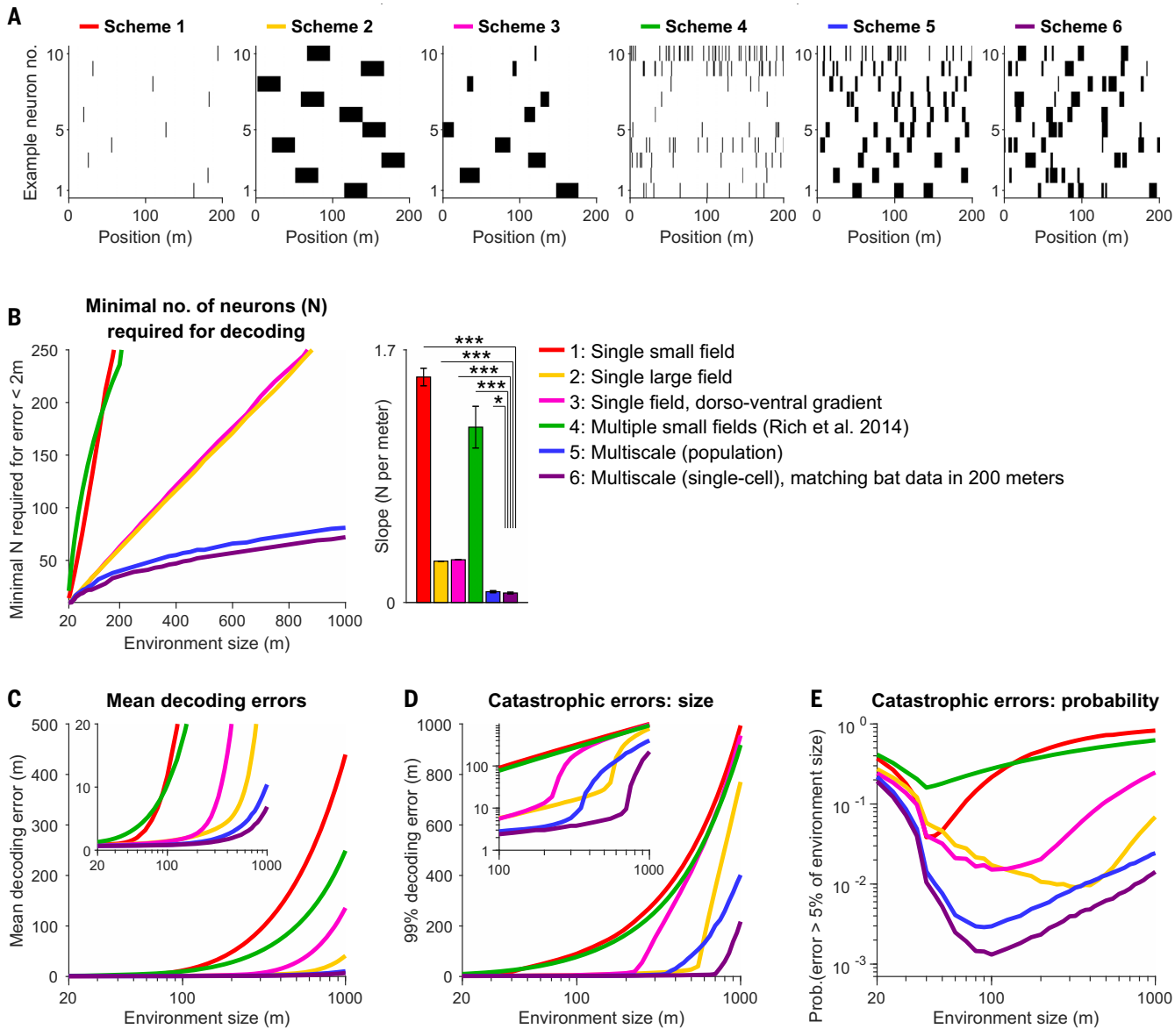

Fig. 7. Theoretical analysis showed that multiscale coding decreases the decoding error for large environments. Decoding accuracy analysis for simulations of six different models (encoding schemes), using maximum likelihood decoder and integration time window of 500 ms (*27*). (**A**) We examined six different encoding schemes for spatial representations; shown here are 10 simulated example neurons for each scheme: (scheme 1) single field with small size; (scheme 2) single field with large size; (scheme 3) single field with gradually increasing field-size across neurons – mimicking the dorso-ventral anatomical gradient of field sizes; (scheme 4) multiple small fields [the distribution of field-propensity was taken from (*18*)]; (scheme 5) multiple fields with fixed size per neuron, but with variable sizes across the population; and (scheme 6) multiple fields with multiscale per neuron (as in the bat data). In schemes 5 and 6, we matched the distribution of field sizes to our data (fig. S8). The mean coverage in schemes 2, 5, and 6 was identical (*27*). (**B**) (Left) Minimal number of neurons required for reaching mean decoding error <2 m, plotted as a function of different environment sizes (from 20 to 1000 m). (Right) Slopes of the curves on the left, representing how many additional neurons are required on average when increasing the environment size by 1 m. Colors represent the six encoding schemes. (**C** to **E**) Decoding errors when using $n = 50$ neurons. (C) Mean decoding error versus environment size, showing that schemes 1, 3, and 4 exhibit huge decoding errors for large environments. (Inset) Zoom-in on errors smaller than 20 m (y axis), showing that per-neuron multiscale encoding (scheme 6, purple) outperforms fixed scale per-neuron (scheme 5, blue) in terms of mean decoding error. [(D) and (E)] Catastrophic errors. (D) Rare large errors (99th percentile of decoding error), plotted versus environment size. (Inset) Same plot in log-scale for the y axis. (E) Probability of decoding error larger than 5% of the environment size, plotted as a function of environment size. (**F**) Theoretical estimate of energy expenditure under the various coding schemes: Shown is the number of ATP molecules per second required to represent the environment with mean decoding error < 2 m, plotted against the environment size (*27*).

coding scheme with a set of five other coding schemes, we generated synthetic data for each coding scheme and then used maximum-likelihood and population-vector decoders to test their decoding performance. To theoretically explore the possible neural-network mechanisms underlying the observed coding, we considered both an attractor network model, based on multiple interacting attractors that randomly share neurons between them, as well as four feedforward models, based on inputs from MEC and CA3. Further details can be found in the supplementary materials, materials and methods.

REFERENCES AND NOTES

1. J. O'Keefe, J. Dostrovsky, The hippocampus as a spatial map. Preliminary evidence from unit activity in the freely-moving rat. *Brain Res.* **34**, 171–175 (1971). doi: 10.1016/0006-8993(71)90358-1; pmid: 5124915
2. J. O'Keefe, L. Nadel, *The Hippocampus as a Cognitive Map* (Oxford Univ. Press, 1978).
3. P. Andersen, R. G. M. Morris, D. G. Amaral, T. V. Bliss, J. O'Keefe, Eds., *The Hippocampus Book* (Oxford Univ. Press, 2007).
4. J. B. Ranck Jr., Head direction cells in the deep layer of dorsal presubiculum in freely moving rats. *Soc. Neurosci. Abstr.* **10**, 599 (1984).
5. J. S. Taube, R. U. Muller, J. B. Ranck Jr., Head-direction cells recorded from the postsubiculum in freely moving rats. I. Description and quantitative analysis. *J. Neurosci.* **10**, 420–435 (1990). doi: 10.1523/JNEUROSCI.10-02-00420.1990; pmid: 2303851
6. T. Hafting, M. Fyhn, S. Molden, M.-B. Moser, E. I. Moser, Microstructure of a spatial map in the entorhinal cortex. *Nature* **436**, 801–806 (2005). doi: 10.1038/nature03721; pmid: 15965463
7. C. Barry, R. Hayman, N. Burgess, K. J. Jeffery, Experience-dependent rescaling of entorhinal grids. *Nat. Neurosci.* **10**, 682–684 (2007). doi: 10.1038/nn1905; pmid: 17486102
8. T. Solstad, C. N. Boccara, E. Kropff, M.-B. Moser, E. I. Moser, Representation of geometric borders in the entorhinal cortex. *Science* **322**, 1865–1868 (2008). doi: 10.1126/science.1166466; pmid: 19095945
9. C. Lever, S. Burton, A. Jeewajee, J. O'Keefe, N. Burgess, Boundary vector cells in the subiculum of the hippocampal formation. *J. Neurosci.* **29**, 9771–9777 (2009). doi: 10.1523/JNEUROSCI.1319-09.2009; pmid: 19657030
10. E. I. Moser, M.-B. Moser, B. L. McNaughton, Spatial representation in the hippocampal formation: A history. *Nat. Neurosci.* **20**, 1448–1464 (2017). doi: 10.1038/nn.4653; pmid: 29073644
11. M. A. Wilson, B. L. McNaughton, Dynamics of the hippocampal ensemble code for space. *Science* **261**, 1055–1058 (1993). doi: 10.1126/science.8351520; pmid: 8351520
12. S. Leutgeb *et al.*, Independent codes for spatial and episodic memory in hippocampal neuronal ensembles. *Science* **309**, 619–623 (2005). doi: 10.1126/science.1114037; pmid: 16040709
13. C. D. Harvey, F. Collman, D. A. Dombeck, D. W. Tank, Intracellular dynamics of hippocampal place cells during virtual navigation. *Nature* **461**, 941–946 (2009). doi: 10.1038/nature08499; pmid: 19829374
14. S. Royer, A. Sirota, J. Patel, G. Buzsáki, Distinct representations and theta dynamics in dorsal and ventral hippocampus. *J. Neurosci.* **30**, 1777–1787 (2010). doi: 10.1523/JNEUROSCI.4681-09.2010; pmid: 20130187
15. I. Lee, D. Yoganarasimha, G. Rao, J. J. Knierim, Comparison of population coherence of place cells in hippocampal subfields CA1 and CA3. *Nature* **430**, 456–459 (2004). doi: 10.1038/nature02739; pmid: 15229614
16. J. K. Leutgeb, S. Leutgeb, M.-B. Moser, E. I. Moser, Pattern separation in the dentate gyrus and CA3 of the hippocampus. *Science* **315**, 961–966 (2007). doi: 10.1126/science.1135801; pmid: 17303747
17. K. B. Kjelstrup *et al.*, Finite scale of spatial representation in the hippocampus. *Science* **321**, 140–143 (2008). doi: 10.1126/science.1157086; pmid: 18599792
18. P. D. Rich, H.-P. Liaw, A. K. Lee, Large environments reveal the statistical structure governing hippocampal representations. *Science* **345**, 814–817 (2014). doi: 10.1126/science.1255635; pmid: 25124440
19. K. D. Taylor, Range of movement and activity of common rats (*Rattus norvegicus*) on agricultural land. *J. Appl. Ecol.* **15**, 663–677 (1978). doi: 10.2307/2402767
20. J. C. Russell, A. J. C. McMorland, J. W. B. MacKay, Exploratory behaviour of colonizing rats in novel environments. *Anim. Behav.* **79**, 159–164 (2010). doi: 10.1016/j.anbehav.2009.10.020
21. M. Geva-Sagiv, L. Las, Y. Yovel, N. Ulanovsky, Spatial cognition in bats and rats: From sensory acquisition to multiscale maps and navigation. *Nat. Rev. Neurosci.* **16**, 94–108 (2015). doi: 10.1038/nrn3888; pmid: 25601780
22. A. Tsoar *et al.*, Large-scale navigational map in a mammal. *Proc. Natl. Acad. Sci. U.S.A.* **108**, E718–E724 (2011). doi: 10.1073/pnas.1107365108; pmid: 21844350
23. N. Ulanovsky, C. F. Moss, Hippocampal cellular and network activity in freely moving echolocating bats. *Nat. Neurosci.* **10**, 224–233 (2007). doi: 10.1038/nn1829; pmid: 17220886
24. M. M. Yartsev, M. P. Witter, N. Ulanovsky, Grid cells without theta oscillations in the entorhinal cortex of bats. *Nature* **479**, 103–107 (2011). doi: 10.1038/nature10583; pmid: 22051680
25. M. M. Yartsev, N. Ulanovsky, Representation of three-dimensional space in the hippocampus of flying bats. *Science* **340**, 367–372 (2013). doi: 10.1126/science.1235338; pmid: 23599496
26. A. Finkelstein *et al.*, Three-dimensional head-direction coding in the bat brain. *Nature* **517**, 159–164 (2015). doi: 10.1038/nature14031; pmid: 25470055
27. Materials and methods are available as supplementary materials.
28. L. T. Thompson, P. J. Best, Place cells and silent cells in the hippocampus of freely-behaving rats. *J. Neurosci.* **9**, 2382–2390 (1989). doi: 10.1523/JNEUROSCI.09-07-02382.1989; pmid: 2746333
29. B. L. McNaughton, C. A. Barnes, J. O'Keefe, The contributions of position, direction, and velocity to single unit activity in the hippocampus of freely-moving rats. *Exp. Brain Res.* **52**, 41–49 (1983). doi: 10.1007/BF00237147; pmid: 6628596
30. M. Geva-Sagiv, S. Romani, L. Las, N. Ulanovsky, Hippocampal global remapping for different sensory modalities in flying bats. *Nat. Neurosci.* **19**, 952–958 (2016). doi: 10.1038/nn.4310; pmid: 27239936
31. A. A. Fenton *et al.*, Unmasking the CA1 ensemble place code by exposures to small and large environments: More place cells and multiple, irregularly arranged, and expanded place fields in the larger space. *J. Neurosci.* **28**, 11250–11262 (2008). doi: 10.1523/JNEUROSCI.2862-08.2008; pmid: 18971467
32. E. Park, D. Dvorak, A. A. Fenton, Ensemble place codes in hippocampus: CA1, CA3, and dentate gyrus place cells have multiple place fields in large environments. *PLOS ONE* **6**, e22349 (2011). doi: 10.1371/journal.pone.0022349; pmid: 21789250
33. G. Buzsáki, K. Mizuseki, The log-dynamic brain: How skewed distributions affect network operations. *Nat. Rev. Neurosci.* **15**, 264–278 (2014). doi: 10.1038/nrn3687; pmid: 24569488
34. J. S. Lee, J. J. Briguglio, J. D. Cohen, S. Romani, A. K. Lee, The statistical structure of the hippocampal code for space as a function of time, context, and value. *Cell* **183**, 620–635 (2020). doi: 10.1016/j.cell.2020.09.024; pmid: 33035454
35. Y. Ziv *et al.*, Long-term dynamics of CA1 hippocampal place codes. *Nat. Neurosci.* **16**, 264–266 (2013). doi: 10.1038/nn.3329; pmid: 23396101
36. A. Rubin, N. Geva, L. Sheintuch, Y. Ziv, Hippocampal ensemble dynamics timestamp events in long-term memory. *eLife* **4**, e12247 (2015). doi: 10.7554/eLife.12247; pmid: 26682652
37. L. Harten, A. Katz, A. Goldshtein, M. Handel, Y. Yovel, The ontogeny of a mammalian cognitive map in the real world. *Science* **369**, 194–197 (2020). doi: 10.1126/science.aay3354; pmid: 32647001
38. S. Hallermann, C. P. J. de Kock, G. J. Stuart, M. H. P. Kole, State and location dependence of action potential metabolic cost in cortical pyramidal neurons. *Nat. Neurosci.* **15**, 1007–1014 (2012). doi: 10.1038/nn.3132; pmid: 22660478
39. D. Zipser, A computational model of hippocampal place fields. *Behav. Neurosci.* **99**, 1006–1018 (1985). doi: 10.1037/0735-7044.99.5.1006; pmid: 3843299
40. M. Tsodyks, T. Sejnowski, Associative memory and hippocampal place cells. *Int. J. Neural Syst.* **6**, 81–86 (1995).
41. J. O'Keefe, N. Burgess, Geometric determinants of the place fields of hippocampal neurons. *Nature* **381**, 425–428 (1996). doi: 10.1038/381425a0; pmid: 8632799
42. A. Samsonovich, B. L. McNaughton, Path integration and cognitive mapping in a continuous attractor neural network model. *J. Neurosci.* **17**, 5900–5920 (1997). doi: 10.1523/JNEUROSCI.17-15-05900.1997; pmid: 9221787
43. F. P. Battaglia, A. Treves, Attractor neural networks storing multiple space representations: A model for hippocampal place fields. *Phys. Rev. E* **58**, 7738–7753 (1998). doi: 10.1103/PhysRevE.58.7738
44. M. Tsodyks, Attractor neural network models of spatial maps in hippocampus. *Hippocampus* **9**, 481–489 (1999). doi: 10.1002/(SICI)1098-1063(1999)9:4<481::AID-HIPO14>3.0.CO;2-S; pmid: 10495029
45. T. Hartley, N. Burgess, C. Lever, F. Cacucci, J. O'Keefe, Modeling place fields in terms of the cortical inputs to the hippocampus. *Hippocampus* **10**, 369–379 (2000). doi: 10.1002/1098-1063(2000)10:4<369::AID-HIPO3>3.0.CO;2-0; pmid: 10985276
46. T. Strösslin, D. Sheynikhovich, R. Chavarriaga, W. Gerstner, Robust self-localisation and navigation based on hippocampal place cells. *Neural Netw.* **18**, 1125–1140 (2005). doi: 10.1016/j.neunet.2005.08.012; pmid: 16263241
47. J. J. Knierim, K. Zhang, Attractor dynamics of spatially correlated neural activity in the limbic system. *Annu. Rev. Neurosci.* **35**, 267–285 (2012). doi: 10.1146/annurev-neuro-062111-150351; pmid: 22462545
48. R. Ben-Yishai, R. L. Bar-Or, H. Sompolinsky, Theory of orientation tuning in visual cortex. *Proc. Natl. Acad. Sci. U.S.A.* **92**, 3844–3848 (1995). doi: 10.1073/pnas.92.9.3844; pmid: 7731993
49. M. W. Jung, S. I. Wiener, B. L. McNaughton, Comparison of spatial firing characteristics of units in dorsal and ventral hippocampus of the rat. *J. Neurosci.* **14**, 7347–7356 (1994). doi: 10.1523/JNEUROSCI.14-12-07347.1994; pmid: 7996180
50. D. J. Foster, M. A. Wilson, Reverse replay of behavioural sequences in hippocampal place cells during the awake state. *Nature* **440**, 680–683 (2006). doi: 10.1038/nature04587; pmid: 16474382
51. K. Diba, G. Buzsáki, Forward and reverse hippocampal place-cell sequences during ripples. *Nat. Neurosci.* **10**, 1241–1242 (2007). doi: 10.1038/nn1961; pmid: 17828259
52. T. J. Davidson, F. Kloosterman, M. A. Wilson, Hippocampal replay of extended experience. *Neuron* **63**, 497–507 (2009). doi: 10.1016/j.neuron.2009.07.027; pmid: 19709631
53. T. Wolbers, J. M. Wiener, Challenges for identifying the neural mechanisms that support spatial navigation: The impact of spatial scale. *Front. Hum. Neurosci.* **8**, 571 (2014). doi: 10.3389/fnhum.2014.00571; pmid: 25140139
54. T. Eliav *et al.*, Data for "Multiscale representation of very large environments in the hippocampus of flying bats". Zenodo (2021). doi: 10.5281/zenodo.4646728

ACKNOWLEDGMENTS

We thank K. D. Harris and A. Treves for suggestions; D. Omer, A. Rubin, T. Stolero, M. Naim, A. Sarel, S. Palgi, and S. Ray for comments on the manuscript; S. Futerman, I. Shulman, B. Pevzner, K. Dor, S. Kodenzik, E. Solomon, C. Cohen, A. Shalev, N. Raish, and L. Hartman for help with bat training; G. Ankaoua and B. Pasmantirer for mechanical designs; A. Tuval for veterinary support; C. Ra'anan and R. Eilam for histology; and G. Brodsky for graphics. **Funding:** This study was supported by research grants to N.U. from the European Research Council (ERC-CoG– NATURAL_BAT_NAV), Deutsche Forschungsgemeinschaft (DFG-SFB 1372), and Yehuda and Judith Bronicki, and by the André Deloro Prize for Scientific Research and the Kimmel Award for Innovative Investigation to N.U.; N.U. is the incumbent of the Barbara and Morris Levinson Professorial Chair in Brain Research. T.E. was supported by the Otto Schwarz Scholarship, the Horowitz KKL-JNF foundation, and by the Maccabim Foundation Excellence Fellowship for PhD students. **Author contributions:** T.E., L.L., and N.U. conceived the initial experiments. T.E., S.R.M., L.L., and N.U. set up experimental systems. T.E., S.R.M., L.L., and N.U. designed experiments. T.E. conducted experiments for dataset 1, and S.R.M. conducted experiments for datasets 2 to 4. T.E. and S.R.M. analyzed the experimental data. L.L. and N.U. guided the data analysis. J.A. and M.T. conducted the theoretical decoding analysis and neural network modeling. G.G. analyzed the energy-decoding tradeoff. T.E. and N.U. wrote the first draft of the manuscript, with major contribution from L.L.; all authors participated in writing and editing of the manuscript. N.U. supervised the project. **Competing interests:** The authors declare no competing interests. **Data and materials availability:** The data and code that support the conclusions of this study are freely accessible online at Zenodo (*54*).

SUPPLEMENTARY MATERIALS

science.sciencemag.org/content/372/6545/eabg4020/suppl/DC1
Materials and Methods
Supplementary Text
Figs. S1 to S23
Table S1
References (*55*–*75*)
MDAR Reproducibility Checklist

View/request a protocol for this paper from *Bio-protocol*.

4 January 2021; accepted 6 April 2021
10.1126/science.abg4020